Supporting Information Available

Assessing the stability of Pd-exchanged sites in zeolites with the aid of a high throughput workflow

Supporting Information

Hassan Aljama[†], Martin Head-Gordon[‡] and Alexis T. Bell[*,†]

[†] Department of Chemical and Biomolecular Engineering, University of California, Berkeley, California

[‡]Department of Chemistry, University of California, Berkeley, California

All energies and xyz coordinates of the optimized geometries are available in the electronic supporting information (ESI). The nomenclature used to tabulate the data is as follow: zeolite name (CHA or BEA) - a number representing structure with a unique Al arrangement - adsorbate name (Pd^{+2}, $Pd^{+}H^{+}$, Pd^{+}, H^{+} or $H^{+}H^{+}$) - a number representing an initial position of the adsorbate - level of theory (GGA or hGGA) - type of calculations (opt for optimization and sp for single point calculation).

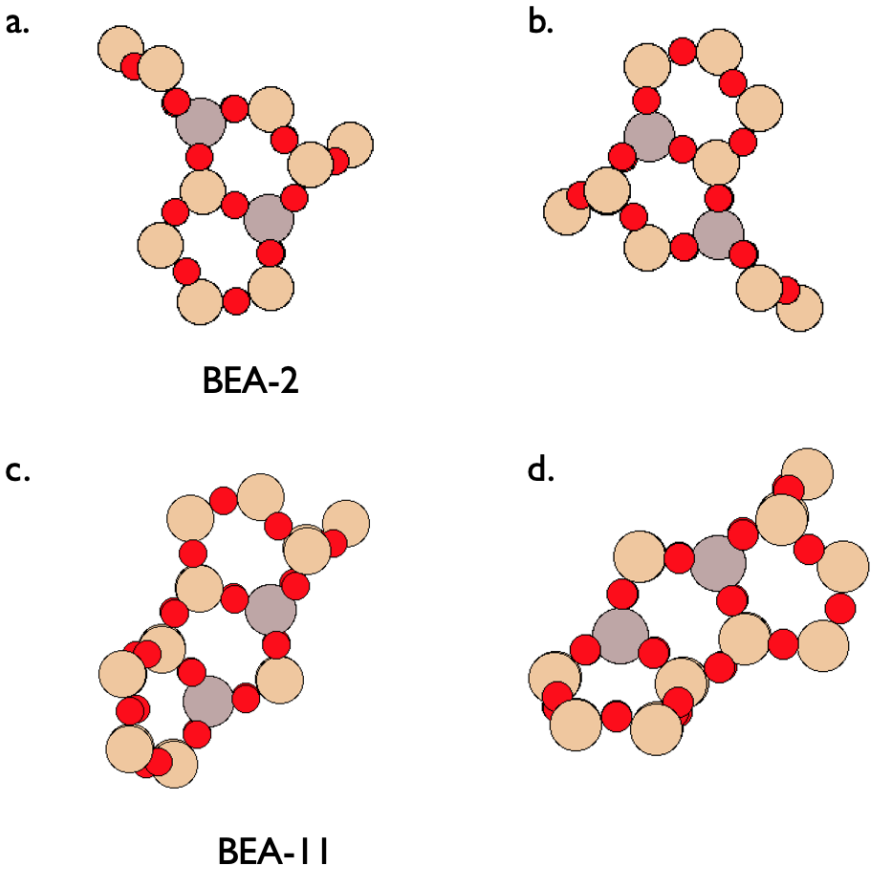

Figure S1: Images of the QM atoms in four BEA structures. BEA-2 structure is shown in a. alongside a similar structure in b. BEA-11 is shown in c. alongside a similar structure in d. The structures similar to BEA-2 and BEA-11 (b. and d., respectively) are not exactly identical, as calculated by the nuclear repulsion energy, but share the same connectivity to surrounding Si and O atoms (types of MR). The same color coding as in Figure 5.

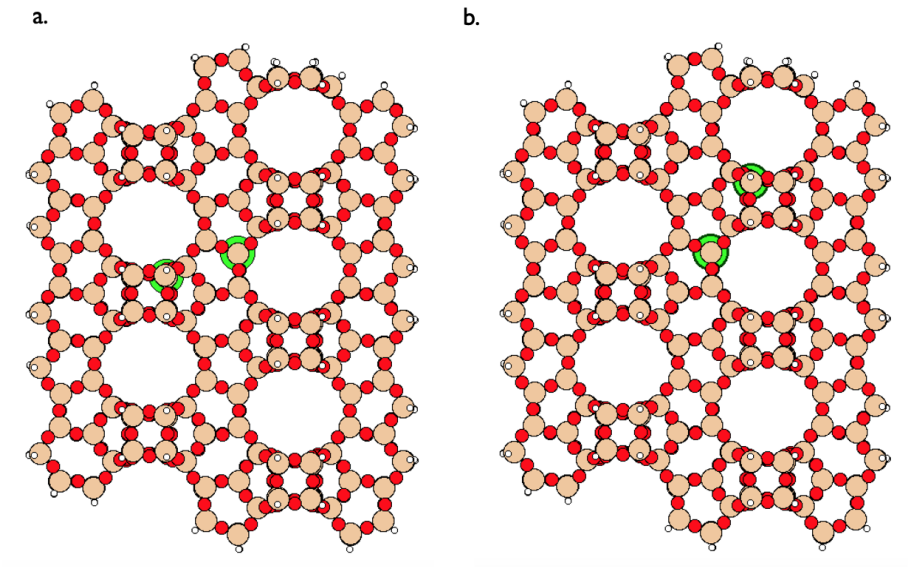

Figure S2: Example of two BEA clusters (a. and b.) where Al atoms are not in the same MR and are on opposite sides of the open cage. The same color coding as in Figure 5, however, for clarity purposes, Al atoms are enlarged and are shown in green

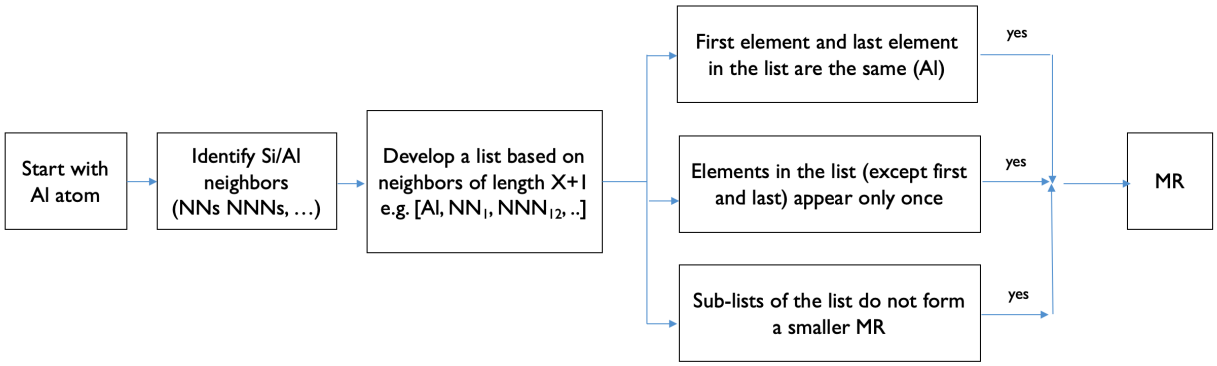

Figure S3: Flow diagram for determining if Al atom is in an X MR (where X refers to the length of the MR). First, starting with an Al atom, Si/Al neighbors (NN, NNN, NNNN) are identified similar to the procedure described in Figure 2. This is done up to the X+1 neighbor. Based on the neighbors, lists are developed (an example of a list is [Al, NN_1, NNN_{11}, ..], where NN_1 refers to the first NN of the starting Al and NNN_{11} is the first NN to NN_1). For each list, the following checks are made: first and last element of the list are the same (the starting Al atom), no element in the list (with the exception of the starting Al atom) appears twice in the list, and no sub-list of the list form a MR smaller than X. If a list passes those checks, then Al is part of XMR.

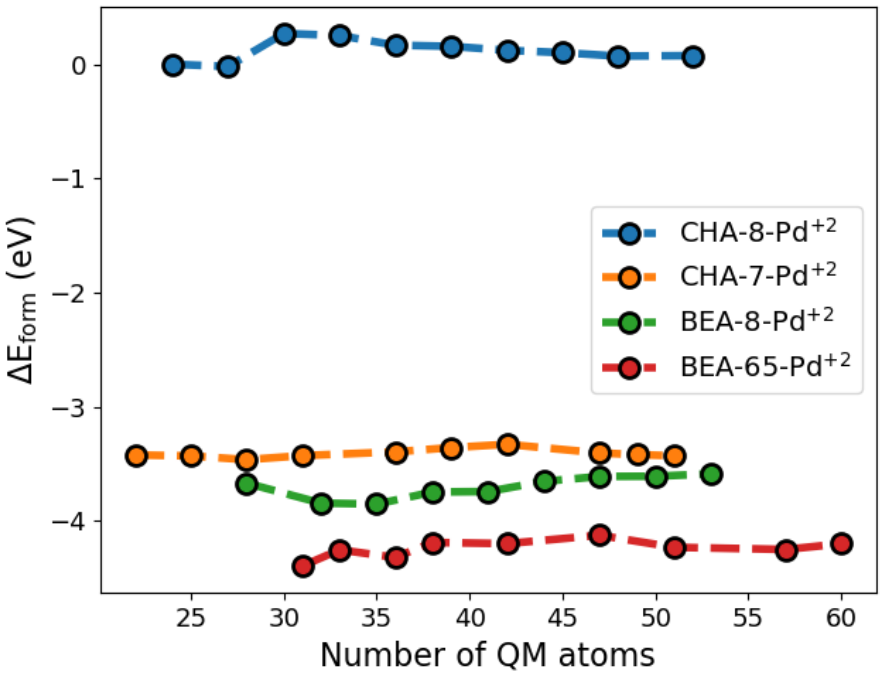

Figure S4: Impact of the number of atoms selected in the QM region on the convergence of the QM/MM calculations (ΔE_{form} is defined in equation 2). Calculations were done using ωB97X-D functional.

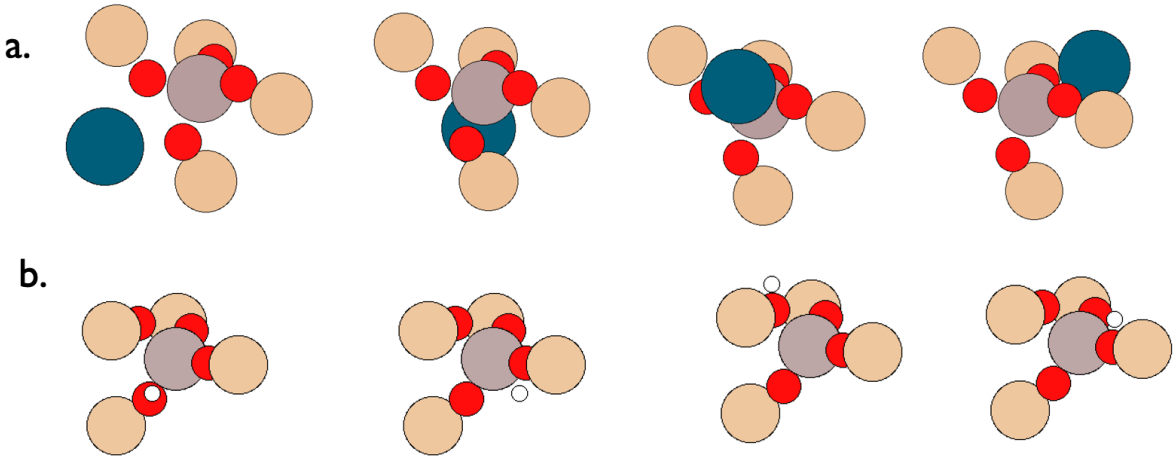

Figure S5: Example of a. Pd cation and b. proton placement near the four oxygens neighboring Al atom. For clarity, only Si in NN position and O neighboring Al are shown. The position of cation/proton is determined by finding the middle distance between neighboring oxygen, and then adding a displacement from the Al atom (usually 1-1.5 A). The same color coding as in Figure 5.

Table S1: Comparison of the stability order (from most stable to 5th most stable) on 3 different structures (BEA-9, BEA-52 and BEA-6) at two levels of theory (GGA and hGGA). The adsorbate is Pd^+H^+. For simplicity, only the 5 most stable structures are shown out of the 32. The two results do not always yield the same order, however, the most stable structure at the hGGA level always appears among the 5 most stable structures at the GGA level. This means following the approach in Figure 1 yields the same results as doing all the calculations using ωB97X-D.

Stability	Theory Level	BEA-9	BEA-52	BEA-63
1st	GGA	BEA-9-Pd^+H^+-3	BEA-52-Pd^+H^+-24	BEA-63-Pd^+H^+-26
	hGGA	BEA-9-Pd^+H^+-12	BEA-52-Pd^+H^+-24	BEA-63-Pd^+H^+-25
2nd	GGA	BEA-9-Pd^+H^+-11	BEA-52-Pd^+H^+-4	BEA-63-Pd^+H^+-25
	hGGA	BEA-9-Pd^+H^+-11	BEA-52-Pd^+H^+-23	BEA-63-Pd^+H^+-26
3rd	GGA	BEA-9-Pd^+H^+-12	BEA-52-Pd^+H^+-3	BEA-63-Pd^+H^+-5
	hGGA	BEA-9-Pd^+H^+-3	BEA-52-Pd^+H^+-1	BEA-63-Pd^+H^+-5
4th	GGA	BEA-9-Pd^+H^+-24	BEA-52-Pd^+H^+-27	BEA-63-Pd^+H^+-24
	hGGA	BEA-9-Pd^+H^+-24	BEA-52-Pd^+H^+-27	BEA-63-Pd^+H^+-24
5th	GGA	BEA-9-Pd^+H^+-27	BEA-52-Pd^+H^+-1	BEA-63-Pd^+H^+-16
	hGGA	BEA-9-Pd^+H^+-27	BEA-52-Pd^+H^+-4	BEA-63-Pd^+H^+-16

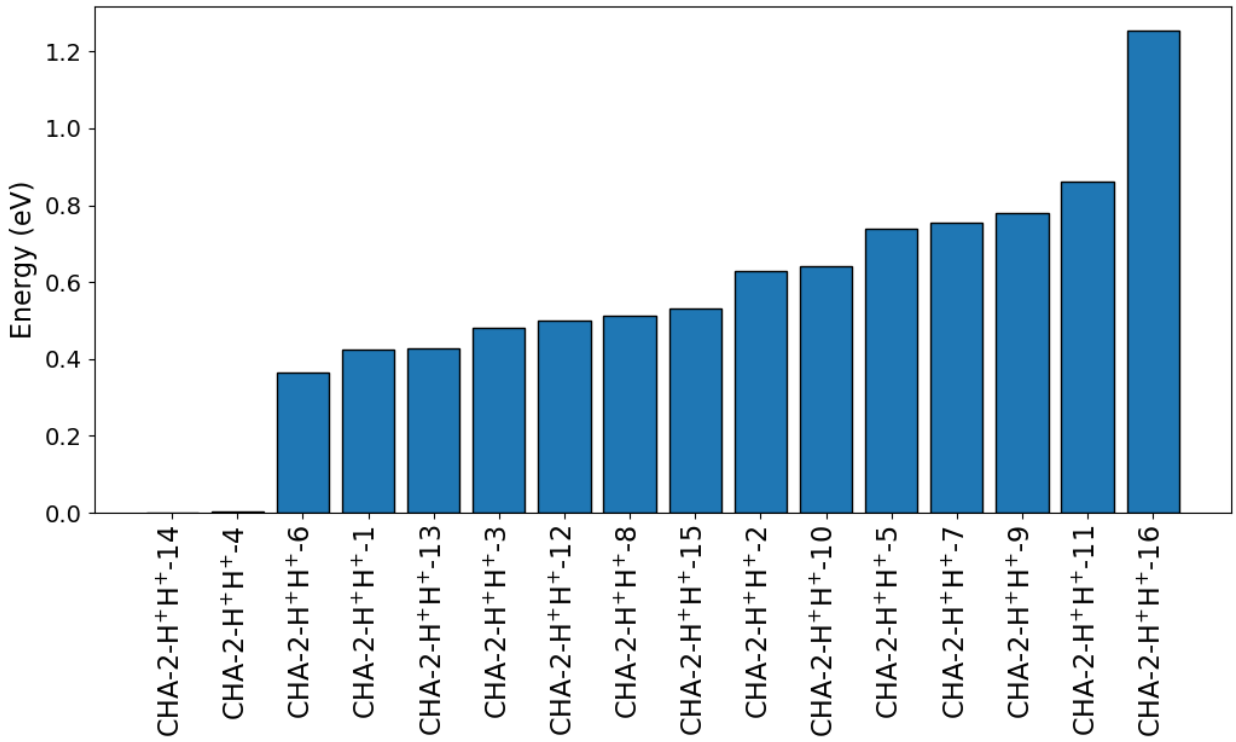

Figure S6: CHA-2 optimum proton locations search results. Each data represents the optimum energy based on a different initial position of the protons. The x-axis refers to the index of the structure in the database in the SI and the y-axis is the energy relative to the most stable structure (CHA-2-H^+H^+-14). Calculations were done using the ωB97X-D functional.

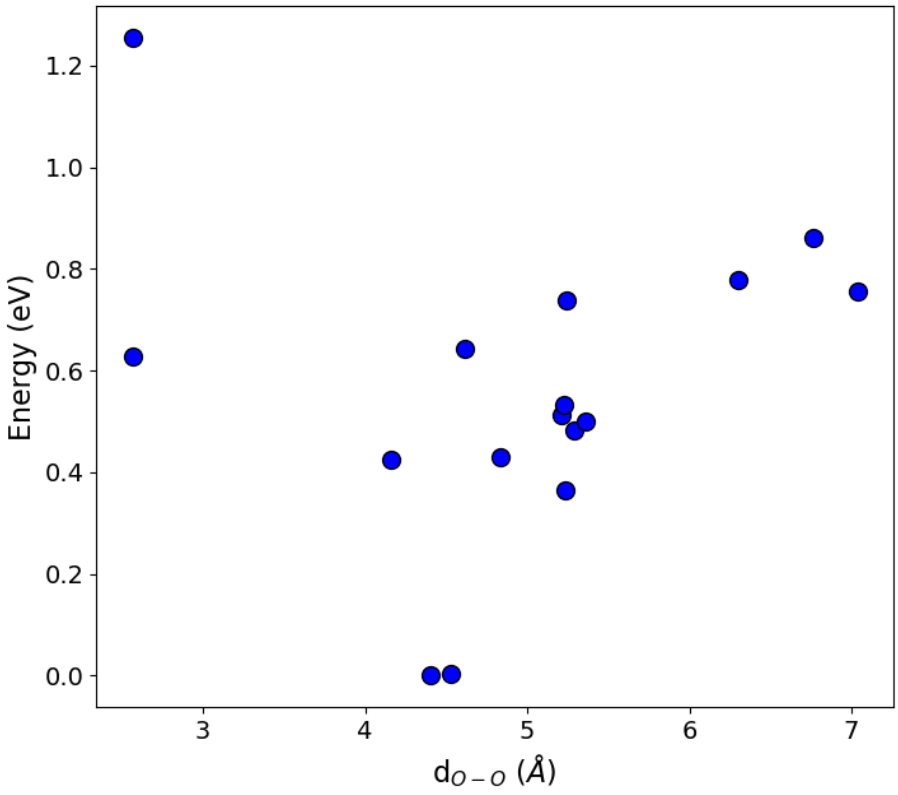

Figure S7: CHA-2 optimum proton locations search results. Each data represents a different initial position of the proton. The x-axis refers to the O-O distance (where the oxygen is the atom H adsorbs on) in the optimized structure and the y-axis is the energy relative to the most stable structure (CHA-2-H^+H^+-14)

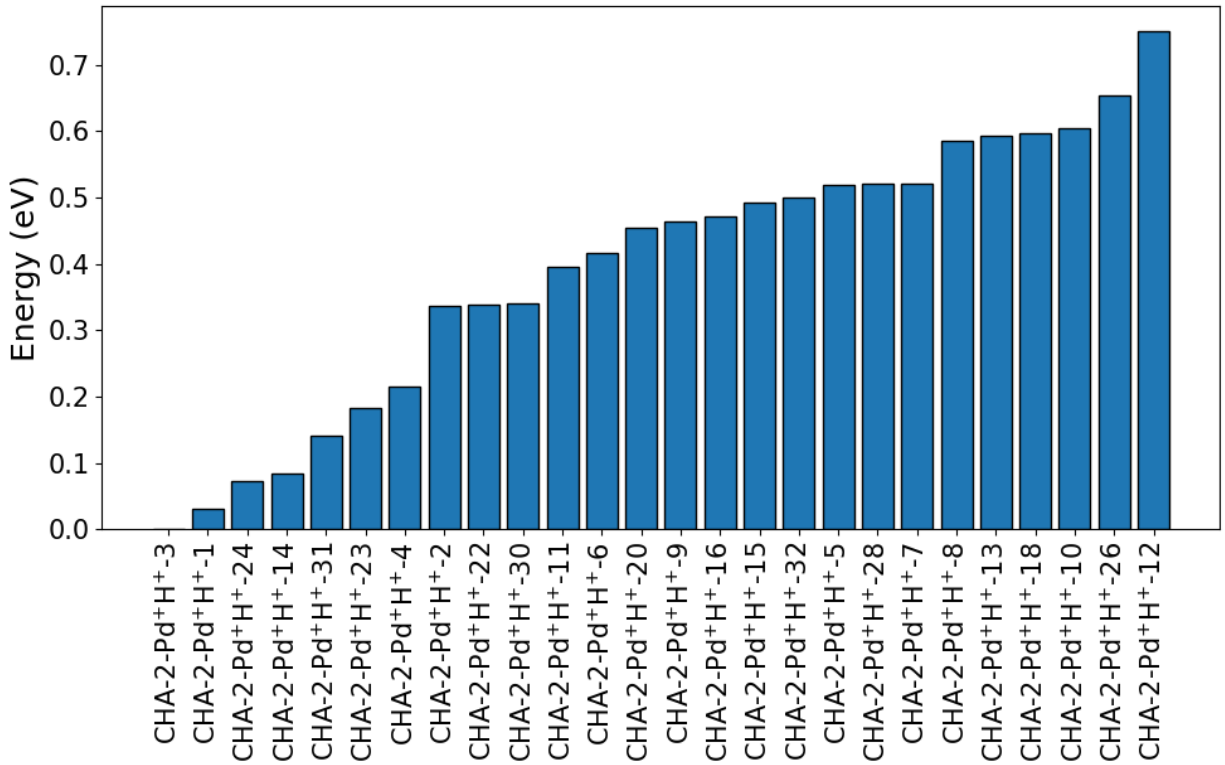

Figure S8: CHA-2 optimum Pd^+H^+ locations search results. Each data represents a different initial position of Pd^+H^+. The x-axis refers to the index of the structure in the database and the y-axis is the energy relative to the most stable structure (CHA-2-Pd^+H^+-3). Calculations were done using the ωB97X-D functional.

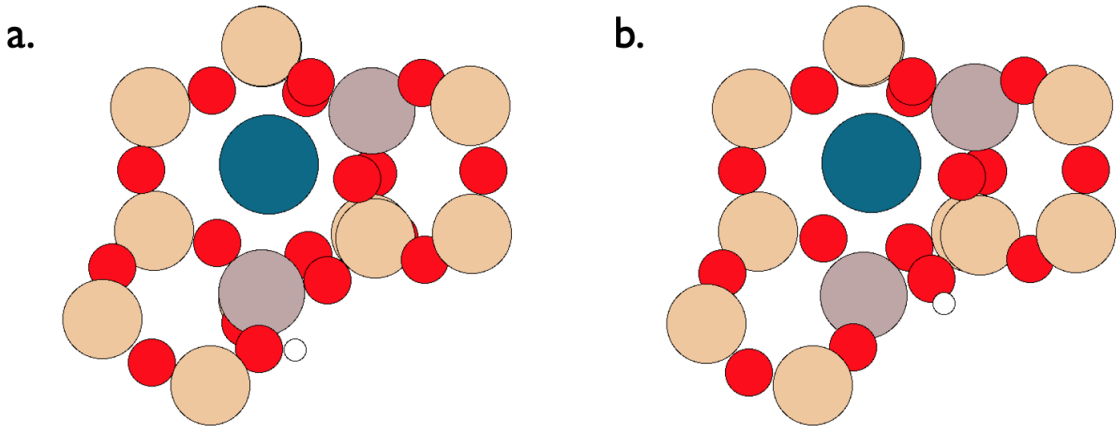

Figure S9: QM images of the optimized geometry of a. CHA-3-$Pd^{+}H^{+}$-21 and b. CHA-3-$Pd^{+}H^{+}$-17. Despite only a change in the proton position, there is >0.4 eV in energy difference between the two optimized geometries. The same color coding as in Figure 5

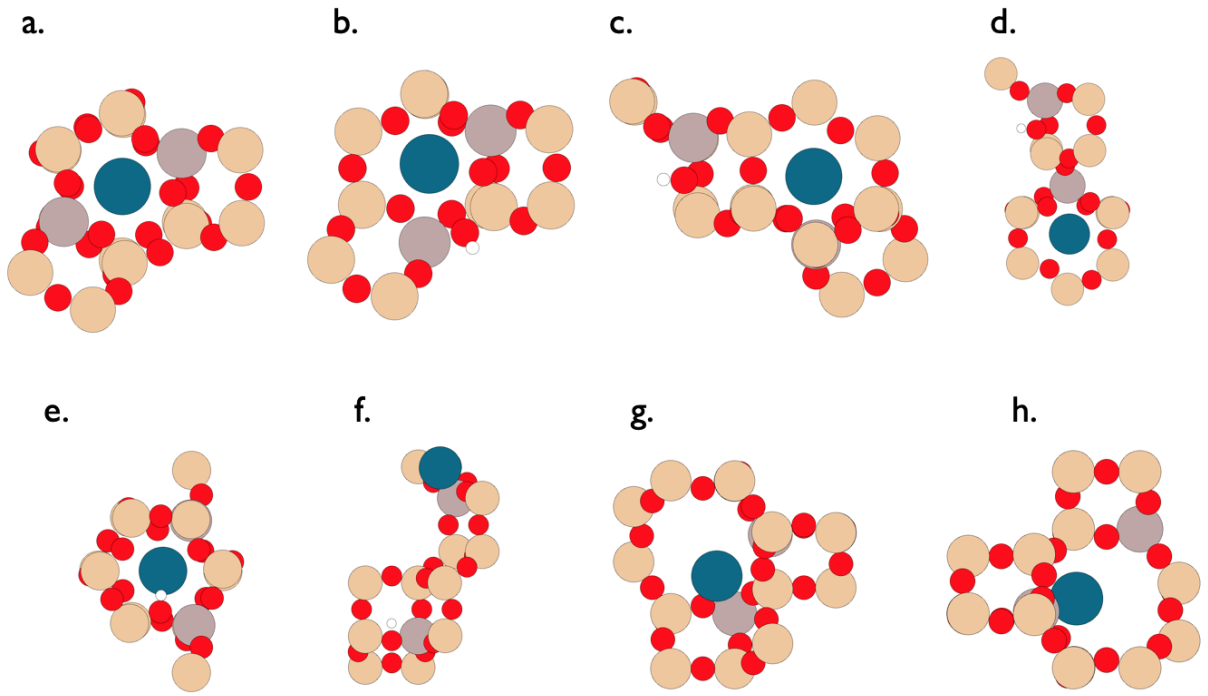

Figure S10: QM region images of the optimized geometry of a. $Pd^{+}H^{+}$ on CHA-7 b. $Pd^{+}H^{+}$ on CHA-3 c. $Pd^{+}H^{+}$ on CHA-8 d. $Pd^{+}H^{+}$ on CHA-6 e. $Pd^{+}H^{+}$ on CHA-9 f. $Pd^{+}H^{+}$ on CHA-12 g. Pd^{+2} on CHA-5 and h. Pd^{+2} on CHA-10. The same color coding as in Figure 5.

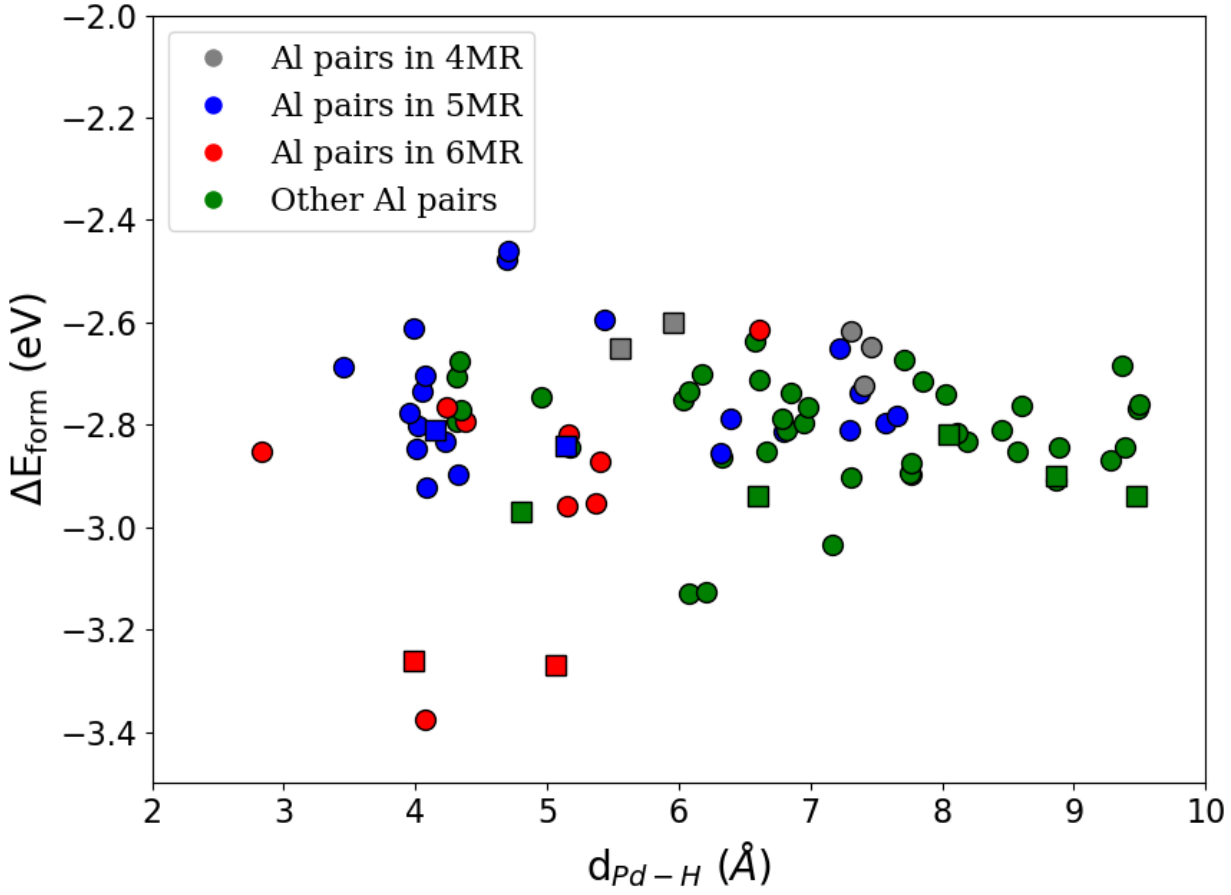

Figure S11: ΔE_{form} as a function of the distance between Pd and H in $Pd^{+}H^{+}$ optimized geometry on CHA (□) and BEA (○)

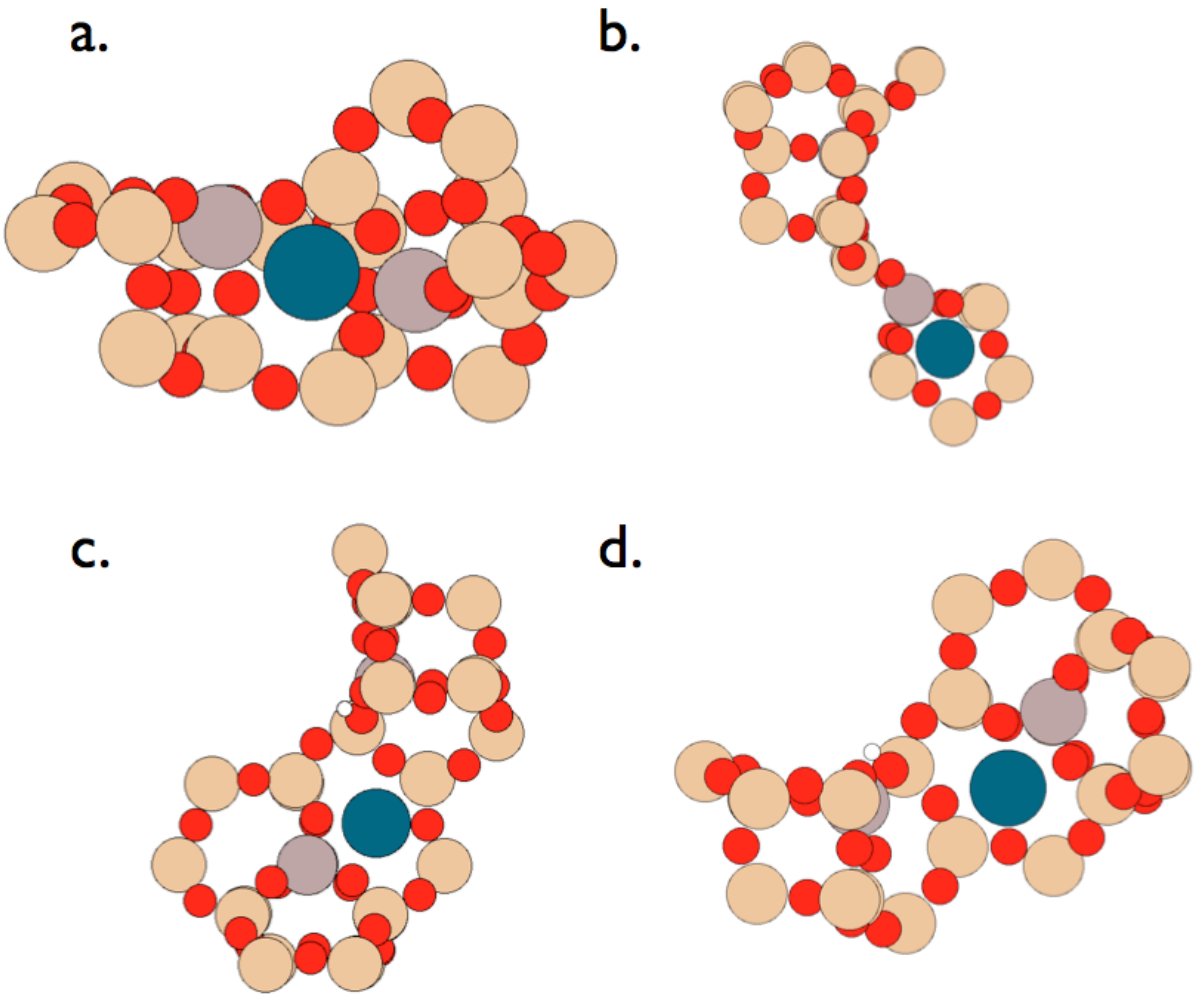

Figure S12: QM region images of optimized geometry of a. Pd^{+2} on BEA-8 b. Pd^{+2} on BEA-55 c. $Pd^{+}H^{+}$ on BEA-33 d. $Pd^{+}H^{+}$ on BEA-55. The same color coding as in Figure 5.

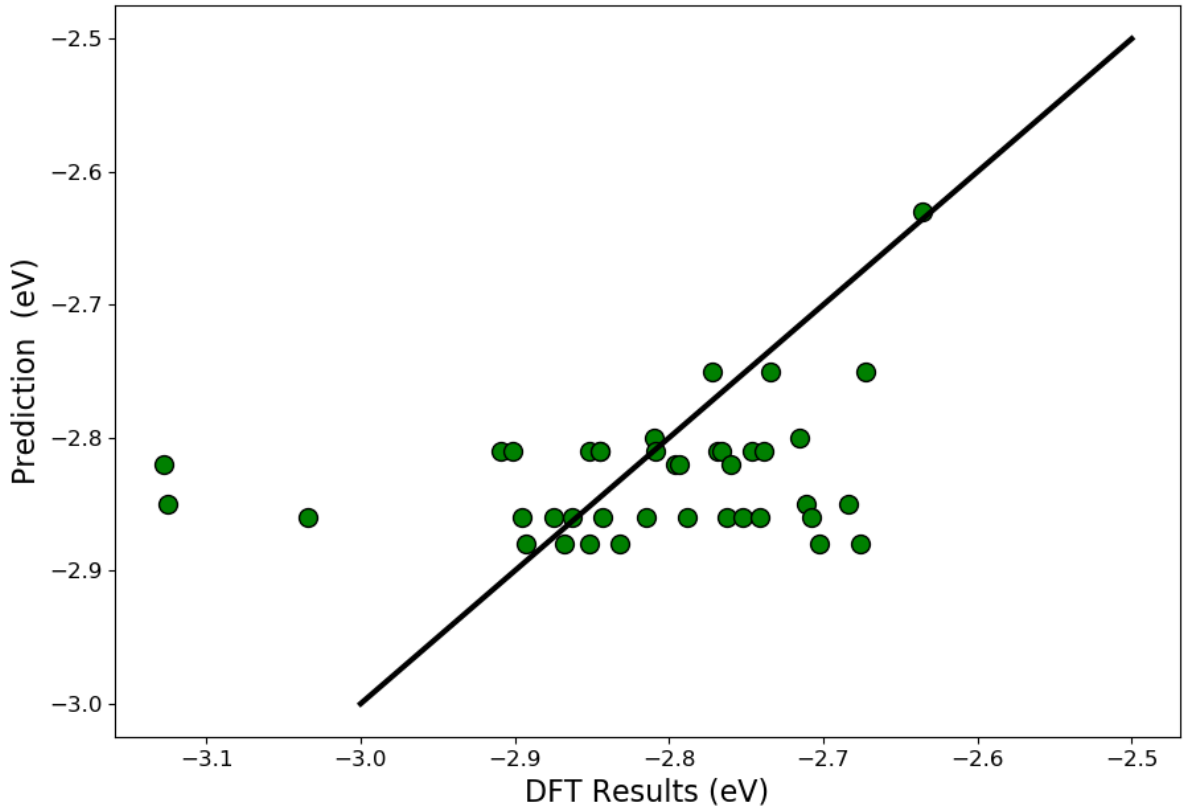

Figure S13: Parity plot of the calculated DFT energy on Al pairs (that do not share a MR) and the predicted energy based on the respective isolated Al site (the most stable of the two). All calculations were done on BEA with $Pd^{+}H^{+}$ as the cation

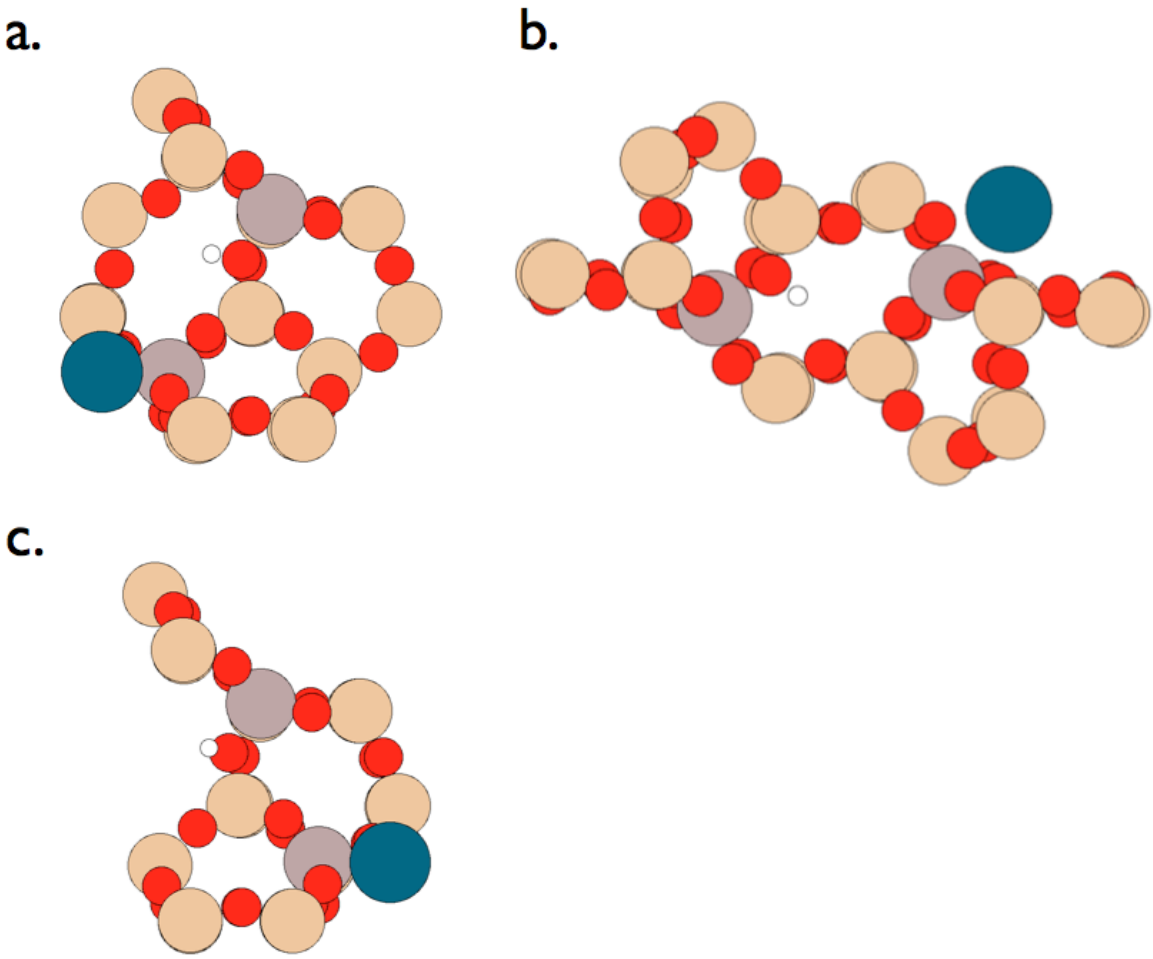

Figure S14: Image of the QM region on optimized BEA calculations a. BEA-51 ($Pd^{+}H^{+}$) b. BEA-78 ($Pd^{+}H^{+}$) c. BEA-52 ($Pd^{+}H^{+}$). The same color coding as in Figure 5.

Table S2: Difference in NO adsorption energy (ΔE_{NO}) on Pd^+H^+ in CHA when the two electrons (from Pd^+ and NO) are paired and the two electrons are unpaired. Paired electrons are used as the reference (0 eV)

Structure Name	Paired Electrons	Two Unpaired Electrons
CHA-5	0	0.89
CHA-8	0	0.82
CHA-7	0	1.53

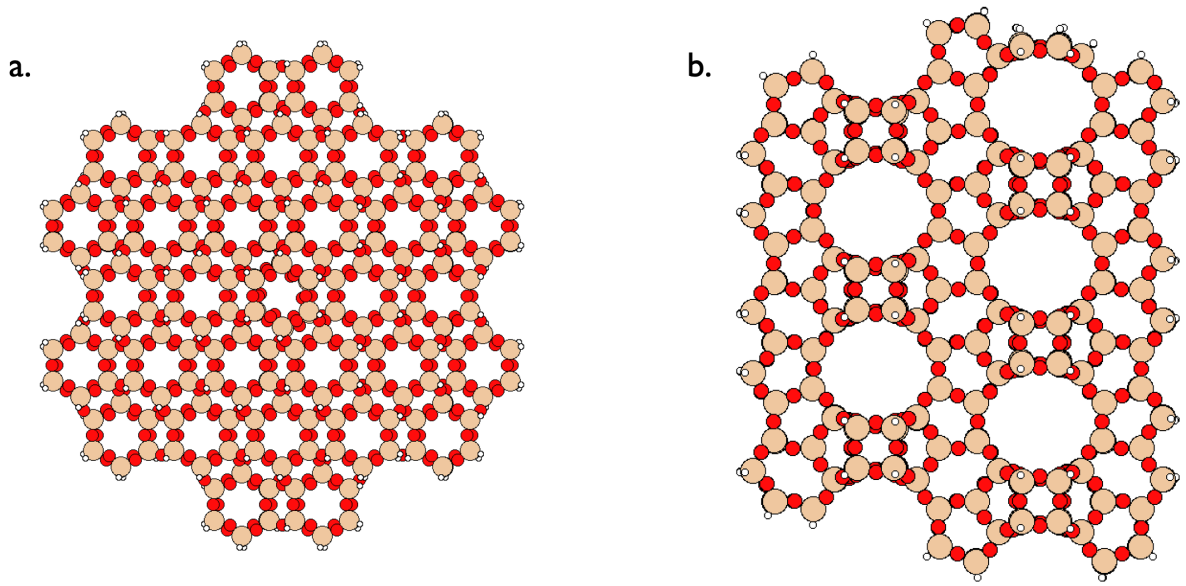

Figure S15: Cluster models of a. T696 CHA and b. T810 BEA. The same color coding as in Figure 5

.